

Double hexameric ring assembly of the type III protein translocase ATPase HrcN

Shirley A. Müller,¹ Charalambos Pozidis,²
Remington Stone,³ Christian Meesters,³
Mohamed Chami,¹ Andreas Engel,¹
Anastassios Economou² and Henning Stahlberg^{3*}

¹M. E. Müller Institute for Structural Biology, Biozentrum, University of Basel, Klingelbergstrasse 70, CH-4056 Basel, Switzerland.

²Institute of Molecular Biology and Biotechnology, FORTH and Department of Biology, University of Crete, PO Box 1527, GR-711 10 Iraklio, Crete, Greece.

³Molecular and Cellular Biology, University of California at Davis, 1 Shields Avenue, Davis, CA 95616, USA.

Summary

The specialized type III secretion (T3S) apparatus of pathogenic and symbiotic Gram-negative bacteria comprises a complex transmembrane organelle and an ATPase homologous to the F₁-ATPase β subunit. The T3S ATPase HrcN of *Pseudomonas syringae* associates with the inner membrane, and its ATP hydrolytic activity is stimulated by dodecamerization. The structure of dodecameric HrcN (HrcN₁₂) determined to 1.6 nm by cryo-electron microscopy is presented. HrcN₁₂ comprises two hexameric rings that are probably stacked face-to-face by the association of their C-terminal domains. It is 11.5 ± 1.0 nm in diameter, 12.0 ± 2.0 nm high and has a 2.0–3.8 nm wide inner channel. This structure is compared to a homology model based on the structure of the F₁- β -ATPase. A model for its incorporation within the T3S apparatus is presented.

Introduction

Gram-negative bacteria possess several protein translocases, among them the type III secretion (hereafter T3S) apparatus of pathogenic and symbiotic bacteria and the bacterial flagellum (He *et al.*, 2004; Macnab, 2004; Tampakaki *et al.*, 2004). T3S machines are complex macromolecular structures that comprise a 'base' that transverses the bacterial envelope, and an extracellular surface appendage (needle or pilus). The tip of this appendage contacts the eukaryotic host cell. Secretory

substrates (e.g. toxins) are recognized by cytoplasmic secretion-specific chaperones (Feldman and Cornelis, 2003), targeted to the inner membrane (Thomas *et al.*, 2004) and apparently secreted/injected through the hollow channel (diameter ~2.5 nm; Blocker *et al.*, 2001; Marlovits *et al.*, 2004) of the T3S machine (Jin and He, 2001).

An ATPase that is related to the F₁-ATPase β subunit (hereafter F₁ β ; Fan and Macnab, 1996; Auvray *et al.*, 2002; Pozidis *et al.*, 2003; Akeda and Galan, 2004), interacts with the T3S substrates and their chaperones (Gauthier and Finlay, 2003; Akeda and Galan, 2004; Thomas *et al.*, 2004) and is essential for their export (Fan and Macnab, 1996; Auvray *et al.*, 2002; Pozidis *et al.*, 2003; Akeda and Galan, 2004). ATP hydrolysis is stimulated modestly by hexamerization (Akeda and Galan, 2004) and strongly by dodecamerization (Pozidis *et al.*, 2003) of the ATPase. The T3S ATPase binds to membranes (Auvray *et al.*, 2002; Minamino *et al.*, 2003; Akeda and Galan, 2004), forms clusters in the inner membrane (Pozidis *et al.*, 2003) and can be extracted from it natively as a dodecamer (Pozidis *et al.*, 2003). However, ultrastructural studies have so far failed to detect the ATPase attached to the T3S apparatus (Kubori *et al.*, 2000; Blocker *et al.*, 2001; Marlovits *et al.*, 2004). Thus, the structural features of this essential component, and its mechanism and role in T3S protein secretion remain elusive.

Here we present the three-dimensional (3D) structure of the dodecameric form of the T3S ATPase HrcN of *Pseudomonas syringae* pathovar *phaseolicola* (hereafter *P. syringae*) determined by cryo-electron microscopy (cryo-EM) to a resolution of 1.6 nm. This structure is compared to a homology model based on the structure of the rat liver F₁ β (Bianchet *et al.*, 1998; see also Fig. S1). A model for its mode of action is proposed.

Results

Mass measurement by scanning transmission electron microscopy (STEM)

Scanning transmission electron microscopy imaging of the unstained, glycerol-free, frozen-dried dodecameric HrcN (Pozidis *et al.*, 2003) sample revealed particles of various sizes. The mass of 1200 particles was determined

Accepted 2 May, 2006. *For correspondence. E-mail hstahlberg@ucdavis.edu; Tel. (+1) 530 752 8282; Fax (+1) 530 752 3085.

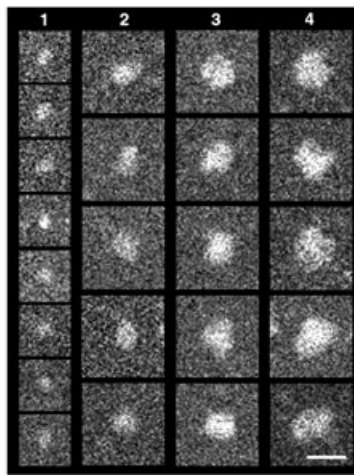
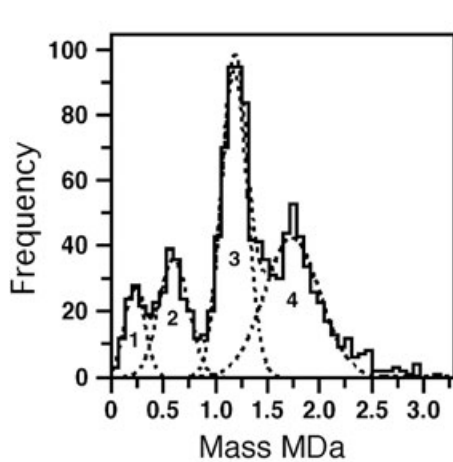


Fig. 1. STEM mass measurements of freeze-dried HrcN complexes. Left. The histogram of the mass values can be described by Gauss curves centred at 225 ± 97 kDa ($n \approx 105$; SE = ± 20 kDa), 601 ± 142 kDa ($n \approx 190$; SE = ± 40 kDa), 1.18 ± 0.13 MDa ($n \approx 472$; SE = ± 75 kDa) and 1.74 ± 0.27 MDa ($n \approx 418$; SE = ± 100 kDa); labelled 1–4 respectively. Right. Typical particles from each peak. Scale bar 20 nm.

and corrected for beam-induced mass-loss. The masses fall into four distinct classes, indicating the presence of complexes composed of 4 ± 2 , 12 ± 3 , 23 ± 3 and 34 ± 5 HrcN monomers (51 kDa each; Fig. 1, peaks 1–4). The peak with the largest population (peak 3) comprises relatively homogeneous particles with diameters approaching 20 nm. Particles in the less populated peak 2 are smaller. While the smallest population (peak 1) probably arises from a minor number of dissociation products, the other peaks are compatible with the presence of dodecamers (12-mer, HrcN₁₂, peak 2) and multiples thereof (24-mers, 36-mers).

Cryo-electron microscopy

Vitrified HrcN₁₂ examined by cryo-EM (Dubochet *et al.*, 1988) revealed densely packed particles (Fig. 2A), with

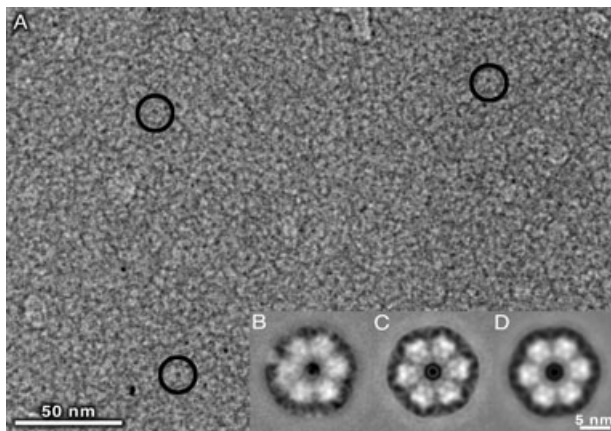


Fig. 2. Cryo-EM imaging of HrcN₁₂ complexes. A. Densely crowded particles in thin ice showing mainly top views (circles). B. Top-view average images. C. The same, sixfold symmetrized. D. The same with applied mirror symmetry, resolution-limited to 0.85 nm.

ring-like projections predominating in thin layers (Fig. 2A, circles; hereafter top view). These were manually selected, reference-free aligned and averaged, yielding a ring-like structure with a clear sixfold symmetry at 0.75 nm resolution (Fig. 2B; Fourier ring correlation, 0.5-criterion; van Heel, 1987; Böttcher *et al.*, 1997). This average image was sixfold symmetrized (Fig. 2C). A copy of this image was then mirrored and aligned onto itself. The two images agreed with each other to 0.85 nm resolution (Fig. 2D). The top-view averages indicate a maximum particle diameter of 12.5 nm and a minimum diameter of 10.3 nm. Less crowded images from thicker ice layers showed random particle orientations, allowing a 3D reconstruction.

A characteristic feature apparent in the top views of HrcN₁₂ is a 2.5 nm wide central 'pore', containing a 1.3 nm wide inner constriction of lower contrast. Side views show this pore to be part of a continuous central channel that crosses HrcN₁₂ longitudinally (Fig. S3).

Three-dimensional reconstruction

The 3D reconstruction of HrcN₁₂ yielded a cylindrical structure 11.5 ± 1.0 nm wide and 12.0 ± 2.0 nm high with ~ 1 nm long spikes projecting from each end, making the total vertical dimension including the spikes 14.0 ± 2.0 nm (Fig. 3A–C). The resolution is 1.6 nm as determined from the Fourier shell correlation function (see *Experimental procedures*). These dimensions, the determined mass (Fig. 1, peak 2; Pozidis *et al.*, 2003) and the sixfold symmetry of the top-view projection maps suggest that the cylinder consists of two HrcN₆ rings stacked on top of one another. The central channel has a maximal diameter of 3.8 nm in the equatorial plane and narrows at the both ends to pores 2 nm in diameter (Fig. 3C).

Three-dimensional maps with the above dimensions were systematically obtained from various starting models

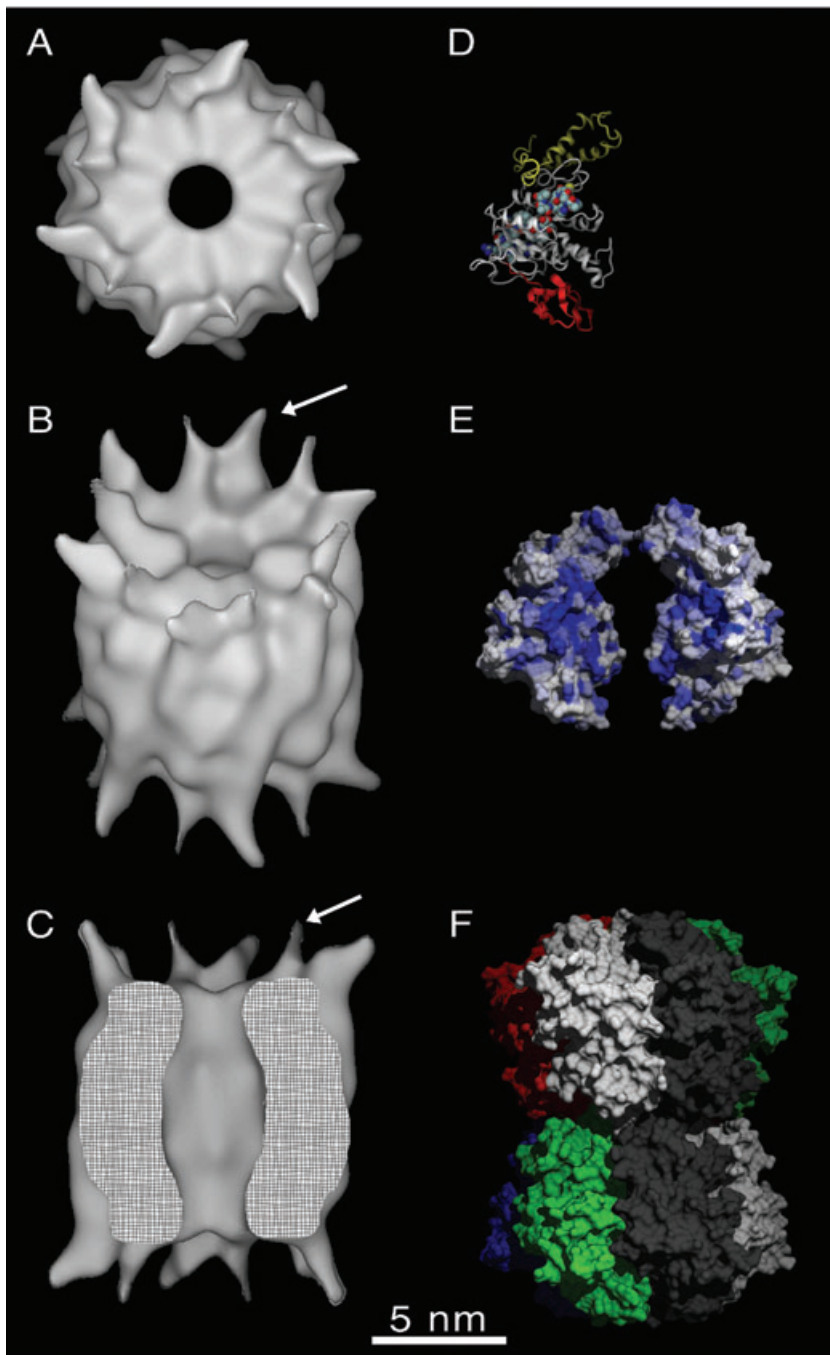


Fig. 3. Three-dimensional reconstruction and model of HrcN.

A–C. 3D reconstruction of the complexes imaged by cryo-EM. The surface threshold was chosen to yield a particle of 612 kDa (using 0.82 kDa nm^{-3}).

A. Top view.

B. Tilted view.

C. Side-view cut along the central axis to reveal the inner channel. Arrows indicate the spikes, see text.

D. Monomeric homology model of HrcN.

N-terminal residues 45–98, red; C-terminal residues 372–448, yellow. The Walker A and B motifs are displayed as van-der-Waals radii.

E. The surface rendered HrcN model coloured according to its sequence conservation (blue = highest, white = lowest). Two opposing monomers from a hexameric assembly are shown.

F. A model of HrcN₁₂ formed from two HrcN₆ complexes, attached face-to-face at their C-terminal ends. The atomic model is compared to the experimental cryo-EM data in Fig. S3.

(Supplementary information online), providing a high degree of confidence in the result. Nevertheless, the possibility that the spike density is originating from the close proximity of neighbouring particles cannot be entirely excluded.

Homology-based 3D model

A homology model for HrcN was generated using the rat liver F₁β (Bianchet *et al.*, 1998) structure (Fig. 3D). The

first 44 residues and the His-tag did not produce a structural motif and were omitted.

The HrcN model was assembled into a hexameric ring using the rotational axis of the F₁ hexamer. The two opposed monomers indicate the shape and dimensions of the channel (Fig. 3E). For this model, conservation is low on the outer surface and the inner channel surface of the complex, as well as in the first 98 (Fig. 3D, red) and in the last 39 residues of the HrcN monomer (Fig. 3D, yellow; Fig. S2). Monomer–monomer interac-

tions are mediated by highly conserved lateral surfaces (Fig. 3D and E, blue).

Discussion

We have structurally characterized the HrcN ATPase, a subunit of the T3S protein translocase of *P. syringae* and present a low-resolution model of the dodecameric form (Fig. 3A–C). To the best of our knowledge this is the first T3S ATPase structure reported.

Cryo-electron microscopy of unstained, frozen hydrated, highly pure HrcN₁₂ immobilized on EM grids immediately after purification, was instrumental to the visualization of the 3D structure. Under these conditions, HrcN₁₂ particles were maintained in stable clusters (Fig. 2). This approach circumvented the tendency of the dodecamers to associate into inactive, higher order aggregates in solution (Pozidis *et al.*, 2003).

Vertically oriented HrcN₁₂ particles had a clear sixfold symmetry (Fig. 2B). This symmetry together with the mass of ~600 kDa (Fig. 1A; peak 2) strongly implies that HrcN₁₂ is formed from two stacked HrcN₆ rings. Based on the near-mirror symmetry of the 2D projection average, we postulate that these rings are stacked 'face-to-face'. Accordingly, the extended longitudinal stacks expected for a 'face-to-back' stacking of HrcN rings were never observed. Moreover, only integral multiples of HrcN₁₂ were identified by STEM mass measurement, and these masses generally arose from side-to-side association of the complexes (Fig. 1).

The 3D reconstruction revealed a cylindrical structure (Fig. 3C) with dimensions compatible with the two-dimensional average map (Fig. 2 insets). The particle height exceeds that of a single HrcN₆ ring and is in agreement with the proposed two-ring assembly model (Fig. S3). The shape of the 3D map and the inability of C-terminal truncated HrcN to form dodecamers while the N-terminally truncated HrcN still does (G. Sianidis, C. Pozidis and A. Economou, unpublished) suggest stacking by association of the C-terminal faces of the two HrcN₆ rings. The dimensions of the homology model based on F₁β and built from two hexameric stacked rings connected at their C-terminal faces (horizontal diameter, 11.8 nm; height, 15 nm; Fig. 3F) also agrees with the diameter (11.5 ± 1.0 nm) and total height (including spikes ~15 nm; Fig. 3C) of the determined 3D map. However, the N-terminal domains of map and model look strikingly different, compatible with the low sequence conservation of the first 98 N-terminal residues and of the residues connecting these to the main part of the HrcN model (Fig. S2). In HrcN this region seems to acquire an extended conformation reaching out from the main body of the structure (Fig. 3C).

Dodecameric forms of the T3S ATPase have been identified in *P. syringae* (Pozidis *et al.*, 2003) and in entero-

pathogenic *Escherichia coli* (C. Pozidis, V. Balabanidou and A. Economou, unpublished). Monomeric and small populations of hexameric (Akeda and Galan, 2004) or dimeric and trimeric (Claret *et al.*, 2003) forms have been identified in other T3S-harboring bacteria. Single particle averaging of projections of negatively stained complexes of Flil revealed ring-shaped structures with six subunits that were stabilized by AMP-PNP (Claret *et al.*, 2003). However, these structures are smaller (outside diameter 10 nm) than those observed here and irregularly shaped. Two pieces of evidence point to the isolated HrcN₁₂ complex being the active form that catalyses T3S translocation: (i) it is hyper-activated for ATP hydrolysis *in vitro* and (ii) it is found associated with membranes (Pozidis *et al.*, 2003). Nevertheless, the possibility that only one of the two HrcN₆ rings is sufficient for translocation *in vivo* cannot be excluded. Future work will discriminate between these two alternatives.

Auxiliary subunits allow the hexameric ring-shaped ATPase motors of several membrane transport systems to specialize in a range of activities, such as transmembrane electrochemical conversions (e.g. the F-ATPases), or transport of DNA (e.g. TrwB) or proteins (e.g. type II or IV secretion systems). F₁-like ATPases have a coiled-coil γ subunit reaching into the F₁-ATPase 'pore', providing a 'stem-like' contact to the membrane-embedded F₀ moiety (Abrahams *et al.*, 1994; Yoshida *et al.*, 2001). In contrast, a γ-like subunit has not been identified in the T3S regulon and the ~2 nm wide channel of the T3S ATPase (Figs 2 and 3) is empty. Furthermore, T3S ATPases are tightly bound to the membrane probably via proteinaceous anchors (Auvray *et al.*, 2002; Pozidis *et al.*, 2003; Akeda and Galan, 2004; Thomas *et al.*, 2004). Accordingly, one exposed N-terminal side of HrcN₁₂ may be involved in membrane assembly, interacting with subunits of the T3S translocase that build the export conduit and the 'base'. In agreement with this, mutations in amino-terminal residues reduce membrane binding of the *Salmonella* InvC homologue (Akeda and Galan, 2004). HrcN₁₂ has a continuous internal channel with end 'pores' 2–3 nm in diameter (Figs 2 and 3). The inner membrane 'base' of various T3S translocases has a transmembrane conduit of similar diameter (2–3 nm) (Ruiz *et al.*, 1993; Blocker *et al.*, 2001) that ends in a membrane-embedded cup-like domain protruding into the cytoplasm (Marlovits *et al.*, 2004). The HrcN₁₂ cylinder has the appropriate external dimensions to fit snugly into this cup and bind to the 'base' to form a continuous putative 'secretion pathway' channel (Fig. 4).

Based on our data we propose the following working hypothesis: (i) the T3S ATPase is a structural component of the T3S translocase, (ii) the T3S ATPase pore aligns with that of the 'base' to form a continuum (Fig. 4), (iii) secretory preproteins migrate through this elongated 'pore', (iv) the 'pore' must be gated and

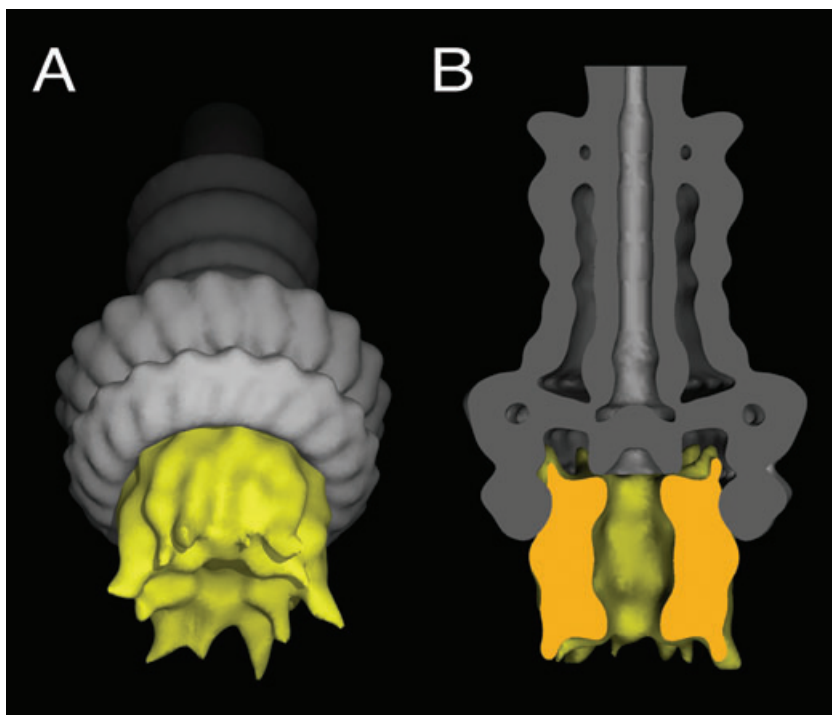


Fig. 4. Model of HrcN₁₂ docked into the needle complex (Marlovits *et al.*, 2004) EmDep Database deposition code EMD-1100).

A. The cryo-EM 3D reconstruction of HrcN₁₂ from *P. syringae* (yellow) fits into the base of the *Salmonella typhimurium* T3S needle complex (grey).

B. The model clipped at its central plane to expose the proposed continuous channel. The figure was generated using Dino (<http://www.dino3d.org>) and POVray (<http://www.povray.org>).

remain closed when inactive, and (v) the T3S ATPase uses ATP hydrolysis to 'pump' the preprotein through the 'pore'. Active release of the preprotein substrate from its chaperone in an ATP hydrolysis-dependent manner (Akeda and Galan, 2004) is expected to be coupled to these processes.

Experimental procedures

Scanning transmission electron microscopy

Scanning transmission electron microscopy grids were prepared from HrcN₁₂ that had been purified as described (Pozidis *et al.*, 2003) but omitting glycerol in the last step (Supplementary information and Fig. S1). A Vacuum Generators STEM HB-5 microscope interfaced to a modular computer system (TVIPS, Gauting, Germany) was employed. Dark-field images were recorded from the frozen-dried unstained sample at 80 kV, using a nominal magnification of 200 000 \times and a recording dose between 220 and 590 electrons nm⁻². Recording of repeated low dose scans allowed the beam-induced mass-loss to be quantified. The images were evaluated using the IMPSYS software (Müller *et al.*, 1992).

Cryo-electron microscopy and image processing

Cryo-electron microscopy grids were prepared from the freshly purified, HrcN₁₂ containing glycerol, within 8 h and imaged using a Philips CM-200-FEG with a Gatan-626 low-temperature holder and low-dose procedures. The presence of glycerol gave a larger time window for optimizing the sample preparation; images recorded from glycerol free samples

looked the same. Recorded micrographs were digitized at 0.2 nm pixel⁻¹ at the specimen level. Defocus and astigmatism were determined using CTFFIND (Grigorieff, 1998). Contrast transfer function (CTF) correction and subsequent processing was carried out with the SPIDER software (Frank *et al.*, 1996).

For the 2D projection map, 2364 projection images were manually selected from a few highly crowded cryo-EM micrographs, windowed, reference-free aligned and averaged. For the 3D reconstruction, 8472 manually selected particle images were reference-free aligned, classified, realigned within each class, and iteratively reassigned to the classes by multi-reference alignment. A first 3D volume was created from a top-view and a side-view class average, applying sixfold rotational (*C*₆) symmetry to the volume. This volume was used as the starting reference for iterative refinement by angular assignment of the 8472 particle images, using reference projections covering the asymmetric triangle, and excluding the particles with the lowest correlation values to the references (5% of the data) in each round. The volume was *C*₆-symmetrized after each round. A stable final volume was reached after seven iterations. This was verified by using different starting models (supplementary information online).

Fourier shell correlation (0.5-criterion) between the volume and a copy of it that had been turned upside down and aligned by rotation around the cylinder axis indicated a resolution of 1.6 nm. At the end of the entire processing, the final volume was averaged with its upside-down rotated copy (*D*₆ symmetry) and resolution limited to 1.6 nm.

Sequence alignment and homology modelling

PIPEALIGN (Plewniak *et al.*, 2003) was used with the sequence of HrcN and other manually selected sequences of

closely related ATPases from the Type III and Type IV secretion machineries. All sequences with a high BLAST-score were included in the alignment. Sequence fragments and repeatedly included or nearly identical sequences were manually removed from the 272 identified. The remaining 185 sequences were aligned.

A structural model was generated based on the homologous rat liver F₁-β-ATPase (25.8% identity, 42.1% similarity; PDB entry 1MAB; Bianchet *et al.*, 1998), using SWISS-MODEL (Schwede *et al.*, 2003).

Acknowledgements

We thank Vesna Olivieri for the STEM microscopy and L. Karamanou for comments. A.En. and A.Ec. were supported by the European Union Directorate of Science and Technology (RTN1-1999-00149), A.Ec. by the Greek Secretariat of Research (AKMON) and A.En. by the Swiss National Foundation (Grant number NF 31-59 415.99) and the Maurice E. Müller Institute of Switzerland. The structure has been deposited at the EmDep Database with Accession code EMD-1160.

References

- Abrahams, J.P., Leslie, A.G., Lutter, R., and Walker, J.E. (1994) Structure at 2.8 Å resolution of F₁-ATPase from bovine heart mitochondria. *Nature* **370**: 621–628.
- Akeda, Y., and Galan, J.E. (2004) Genetic analysis of the *Salmonella enterica* type III secretion-associated ATPase InvC defines discrete functional domains. *J Bacteriol* **186**: 2402–2412.
- Auvray, F., Ozin, A.J., Claret, L., and Hughes, C. (2002) Intrinsic membrane targeting of the flagellar export ATPase FliI: interaction with acidic phospholipids and FliH. *J Mol Biol* **318**: 941–950.
- Bianchet, M.A., Hüllihen, J., Pedersen, P.L., and Amzel, L.M. (1998) The 2.8-Å structure of rat liver F₁-ATPase: configuration of a critical intermediate in ATP synthesis/hydrolysis. *Proc Natl Acad Sci USA* **95**: 11065–11070.
- Blocker, A., Jouihri, N., Larquet, E., Gounon, P., Ebel, F., Parsot, C., *et al.* (2001) Structure and composition of the *Shigella flexneri* 'needle complex', a part of its type III secretion. *Mol Microbiol* **39**: 652–663.
- Böttcher, B., Wynne, S.A., and Crowther, R.A. (1997) Determination of the fold of the core protein of hepatitis B virus by electron cryomicroscopy. *Nature* **386**: 88–91.
- Claret, L., Calder, S.R., Higgins, M., and Hughes, C. (2003) Oligomerization and activation of the FliI ATPase central to bacterial flagellum assembly. *Mol Microbiol* **48**: 1349–1355.
- Dubochet, J., Adrian, M., Chang, J.-J., Homo, J.-C., Lepault, J., McDowell, A.W., and Schultz, P. (1988) Cryo-electron microscopy of vitrified specimens. *Quart Rev Biophys* **21**: 129–228.
- Fan, F., and Macnab, R.M. (1996) Enzymatic characterization of FliI. An ATPase involved in flagellar assembly in *Salmonella typhimurium*. *J Biol Chem* **271**: 31981–31988.
- Feldman, M.F., and Cornelis, G.R. (2003) The multitasking type III chaperones: all you can do with 15 kDa. *FEMS Microbiol Lett* **219**: 151–158.
- Frank, J., Radermacher, M., Penczek, P., Zhu, J., Li, Y., Ladjadi, M., and Leith, A. (1996) SPIDER and WEB: processing and visualization of images in 3D electron microscopy and related fields. *J Struct Biol* **116**: 190–199.
- Gauthier, A., and Finlay, B.B. (2003) Translocated intimin receptor and its chaperone interact with ATPase of the type III secretion apparatus of enteropathogenic *Escherichia coli*. *J Bacteriol* **185**: 6747–6755.
- Grigorieff, N. (1998) Three-dimensional structure of bovine NADH: ubiquinone oxidoreductase (complex I) at 22 Å in ice. *J Mol Biol* **277**: 1033–1046.
- He, S.Y., Nomura, K., and Whittam, T.S. (2004) Type III protein secretion mechanism in mammalian and plant pathogens. *Biochim Biophys Acta* **1694**: 181–206.
- van Heel, M. (1987) Similarity measures between images. *Ultramic* **21**: 95–100.
- Jin, Q., and He, S.Y. (2001) Role of the Hrp pilus in type III protein secretion in *Pseudomonas syringae*. *Science* **294**: 2556–2558.
- Kubori, T., Sukhan, A., Aizawa, S.I., and Galan, J.E. (2000) Molecular characterization and assembly of the needle complex of the *Salmonella typhimurium* type III protein secretion system. *Proc Natl Acad Sci USA* **97**: 10225–10230.
- Macnab, R.M. (2004) Type III flagellar protein export and flagellar assembly. *Biochim Biophys Acta* **1694**: 207–217.
- Marlovits, T.C., Kubori, T., Sukhan, A., Thomas, D.R., Galan, J.E., and Unger, V.M. (2004) Structural insights into the assembly of the type III secretion needle complex. *Science* **306**: 1040–1042.
- Minamino, T., Gonzalez-Pedrajo, B., Kihara, M., Namba, K., and Macnab, R.M. (2003) The ATPase FliI can interact with the type III flagellar protein export apparatus in the absence of its regulator, FliH. *J Bacteriol* **185**: 3983–3988.
- Müller, S., Goldie, K.N., Bürki, R., Häring, R., and Engel, A. (1992) Factors influencing the precision of quantitative scanning transmission electron microscopy. *Ultramic* **46**: 317–334.
- Plewniak, F., Bianchetti, L., Brelivet, Y., Carles, A., Chalmel, F., Lecompte, O., *et al.* (2003) PipeAlign: a new toolkit for protein family analysis. *Nucleic Acids Res* **31**: 3829–3832.
- Pozidis, C., Chalkiadaki, A., Gomez-Serrano, A., Stahlberg, H., Brown, I., Tampakaki, A.P., *et al.* (2003) Type III protein translocase: HrcN is a peripheral ATPase that is activated by oligomerization. *J Biol Chem* **278**: 25816–25824.
- Ruiz, T., Francis, N.R., Morgan, D.G., and DeRosier, D.J. (1993) Size of the export channel in the flagellar filament of *Salmonella typhimurium*. *Ultramic* **49**: 417–425.
- Schwede, T., Kopp, J., Guex, N., and Peitsch, M.C. (2003) SWISS-MODEL: an automated protein homology-modeling server. *Nucleic Acids Res* **31**: 3381–3385.
- Tampakaki, A.P., Fadoulglou, V.E., Gazi, A.D., Panopoulos, N.J., and Kokkinidis, M. (2004) Conserved features of type III secretion. *Cell Microbiol* **6**: 805–816.
- Thomas, J., Stafford, G.P., and Hughes, C. (2004) Docking of cytosolic chaperone-substrate complexes at the membrane ATPase during flagellar type III protein export. *Proc Natl Acad Sci USA* **101**: 3945–3950.

Yoshida, M., Muneyuki, E., and Hisabori, T. (2001) ATP synthase – a marvellous rotary engine of the cell. *Nat Rev Mol Cell Biol* **2**: 669–677.

Supplementary material

The following supplementary material is available for this article online:

Fig. S1. Size exclusion chromatography.

Fig. S2. Conservation within the HrcN sequence alignment.

Fig. S3. Comparison of the experimental cryo-EM data with the atomic model.

This material is available as part of the online article from <http://www.blackwell-synergy.com>